ADVANCED FUNCTIONAL MATERIALS
www.afm-journal.de

A Conformable Holographic Sensing Bandage for Wound Monitoring

Yihan Zhang, Yubing Hu, Yunuen Montelongo, Mintin Hsu, Jeff Blyth, Nan Jiang,* and Ali K. Yetisen**

Chronic wound monitoring can provide personalized pathophysiological information for wound management and treatment. Continuously monitoring the wound milieu via the holographic pH sensor can reflect the wound healing processes. However, the integration with wearable devices is hindered by its inherently restricted interrogation angle dependency within 5°. Herein, a ball bearing-based double photopolymerization method is developed to fabricate holographic pH sensors with a broader interrogation angle range of 15°–60° in wound exudates. The fabricated holographic pH sensor is then integrated with the flexible ultrathin polyurethane substrate, which replays a total Bragg peak shift of approximately 150 nm with physiological pH changes from 7.00 to 8.75. The conformable holographic pH sensing bandages demonstrate the ability to quantify the pH value under various bending manipulations, simulating the mounting on the body surface. The reversibility in artificial wound exudate demonstrates the durability and capability of real-time pH monitoring in the wound milieu with minimal effect on the replay wavelength. The addition of electrolytes, albumin, urea, uric acid, lactate, and glucose does not interfere with the readout over the physiological pH range of wound exudates. The obtained conformable holographic sensing bandage benefits the wound healing process monitoring through colorimetric interrogation at point-of-care (POC) settings.

1. Introduction

The wound healing is closely related to cell metabolism at the wound region and can be affected by various environmental and physiological factors.[1] The wound-healing process can be suppressed by factors such as bacterial colonization and diabetes, resulting in poor healing or chronic wounds. Chronic wounds have become a global economic burden to medical systems in the rapidly aging society. In the United States, over 6.5 million people are affected by chronic wounds, accounting for an annual expense of 25 billion US dollars, emphasizing the high significance of wound monitoring and management.[2] A wound healing process typically includes four continuous overlapping stages: hemostasis, inflammation, proliferation, and remodeling (**Figure 1a**).[3] The healing time of chronic wounds exceeds three months or even fails to experience any normal tissue regeneration process. Long-term exposure to the external environment may even deteriorate the wound milieu and surrounding tissue. However, the current wound assessment heavily relies on clinicians' visual checks and is limited by subjective errors. Conventional biomarker quantification in wound fluids is limited to time-consuming and high-cost lab testing of wound fluids using enzyme-linked immunosorbent assays (ELISAs) that cannot achieve real-time and continuous wound healing monitoring processes.[4] Therefore, a biosensing device that can monitor wound milieu conditions in a non-invasive, continuous, and timely manner is highly desired. Wearable biosensors integrated with wound dressings can quantify wound-healing-related biomarkers, such as pH, glucose, lactate, oxygen, interleukin-6, temperature, and blood

Y. Zhang, Y. Hu, M. Hsu, J. Blyth, A. K. Yetisen
Department of Chemical Engineering
Imperial College London
South Kensington
London SW7 2BU, UK
E-mail: yubing.hu@imperial.ac.uk; a.yetisen@imperial.ac.uk

The ORCID identification number(s) for the author(s) of this article can be found under https://doi.org/10.1002/adfm.202308490

DOI: 10.1002/adfm.202308490

Y. Montelongo
Department of Engineering Science
University of Oxford
Oxford OX1 3PJ, UK

N. Jiang
West China School of Basic Medical Sciences & Forensic Medicine
Sichuan University
Chengdu 610041, China
E-mail: jiangnansophia@scu.edu.cn

N. Jiang
Jinfeng Laboratory
Chongqing 401329, China

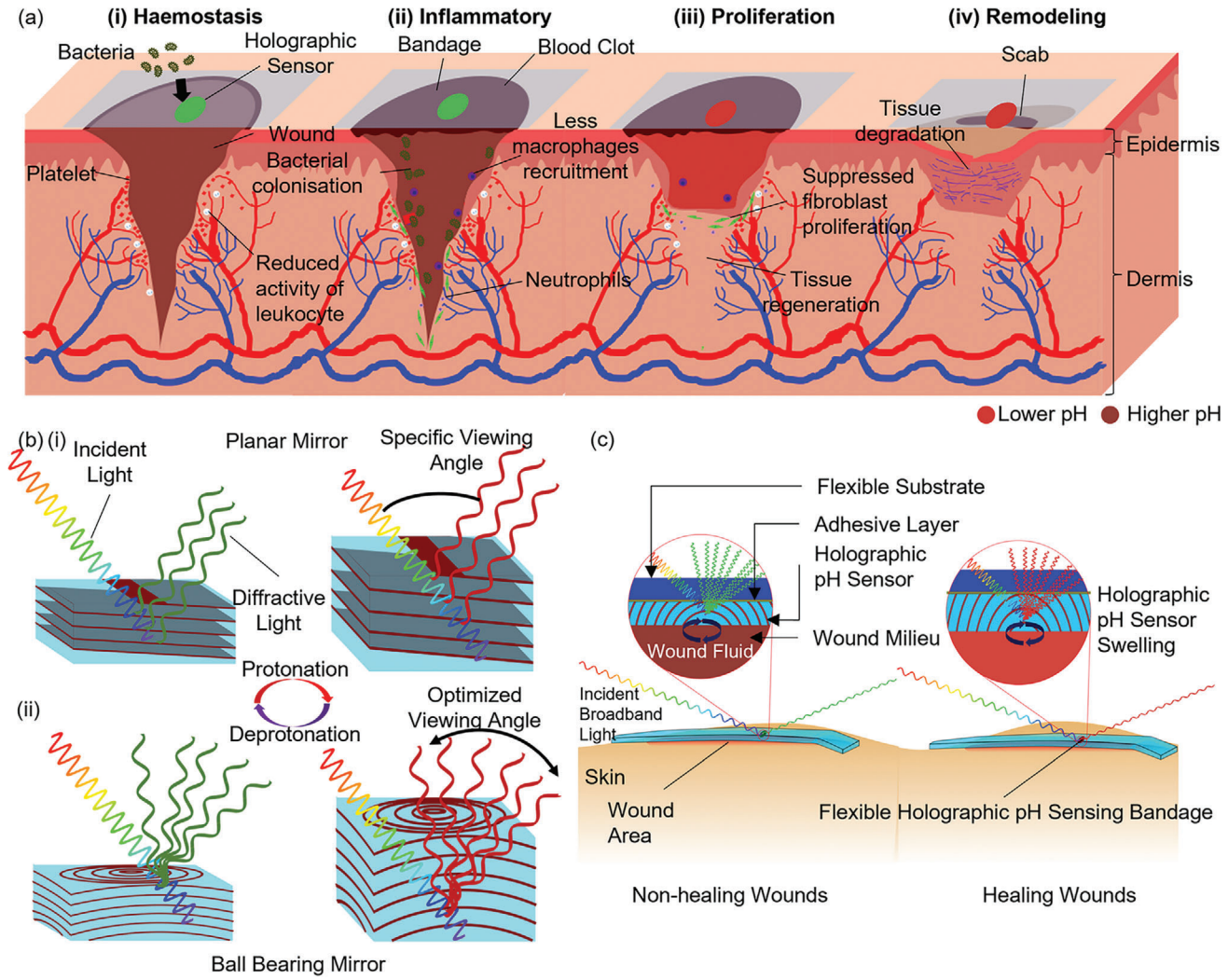

Figure 1. Wound healing monitoring via holographic sensors with a broad viewing angle. a) The impact of alkaline pH of wound exudate in four wound-healing phases i, Haemostasis phase. ii, Inflammatory phase. iii, Proliferation phase. iv, Remodeling phase. b) Comparison in viewing angles of holographic sensors created by light interference from the i, planar mirror and ii, ball-bearing mirror. c) The colorimetric response of holographic pH sensor wearing on non-healing wounds and healing wounds.

pressure, in a non-invasive manner, which has drawn significant attention.[2a,3b,4,5] Wound dressing, such as a bandage, is an effective wearable device to protect wound areas from bacteria-induced infections for a long time, which provides an ideal platform to integrate biosensors in close contact with the wound surface.

pH value variations of wound fluids are closely associated with the wound healing process. For example, protons can intervene in cell metabolism via proton pumps and are involved in critical metabolic reactions such as ATP production and conversion. Protons also modulate protein and enzyme activities by affecting their molecular conformation. In the wound healing process, matrix metalloproteinases and proteases are the most prevalent enzymes modulated by pH values, which delayed the wound healing process at their high activity levels. The pH value of healing wound fluid gradually decreases to a normal skin pH value of 4.0–6.0 as the healing progresses into late proliferation phase, whereas a higher pH value (7.15-8.50) can be found during the inflammatory phase.[6] A long-term inflammatory phase during the wound healing process indicates poor healing or chronic wounds since alkaline pH in the wound exudate would suppress various immune cell activities and fibroblast proliferation, leading to bacterial colonization and tissue degradation at the wound region.[7] Acidification of wound region is a common chronic wound treatment method, and it has been reported to have a potent antibacterial effect and impede extracellular matrix degradation.[6b,8] Therefore, real-time and continuous monitoring of pH value provides an opportunity for early intervention of chronic wounds and precise wound management to facilitate healing and reduce patient suffering. Wearable dressings integrated with various types of electrochemical sensors have been developed to monitor pH values at the wound region.[5a,b,9] For example, a commercial bandage was integrated with a screen-printed silver-silver chloride electrode that could monitor pH changes between 4.35–8.00 with

a signal drift over time.[5b] A multiplexed electrochemical wound healing monitoring microfluidic patch was fabricated to monitor pH, temperature, and protein biomarkers.[5a] However, the requirement of a power source inherently increased the weight and volume of electrochemical sensors. In addition, the power drifting over time during continuous and real-time monitoring indicates a lack of long-term stability. The optical sensor provides good stability over long-term usage, high selectivity towards designated biomarkers, low-cost fabrication, accurate quantification, and easy readout methods, removing the need to use large and complex readout machines.[10] A fluorescent wound sensor was fabricated based on a pyranine-benzalkonium ion pair to monitor pH changes in 5.5–8.5.[11] However, the photobleaching and signal interference might affect the sensing accuracy of the fluorescent sensors. Thus, an unmet need exists to develop long-term stable, power-free, and label-free wearable optical sensors integrated with wound dressings for accurate, real-time, and continuous wound pH monitoring.

Holographic sensors are power-free and label-free photonic crystal sensors that systematically diffract narrow-band light from the ultraviolet to the near-infrared range. These have been widely applied for long-term stable, continuous, reversible, and noninvasive monitoring of physiological biomarkers.[12] A periodic structure of holographic sensors with variations in the refractive index has been constructed by the imprinted grating nanostructure of nanocomposites,[13] nanoparticles,[12d,f,14] or secondary polymer layers.[12c,15] Recently, holographic sensors fabricated by double photopolymerization have been applied in pH sensing with the osmotic and electrostatic force-induced volumetric change of hydrogel.[16] Although the holographic sensor shows potential for biocompatible, reversible, and accurate wound pH monitoring, the inherently narrow range of viewing angles restricts its integration in wearables. This brings complexity to POC applications as patients struggle to find the correct angle to observe the holographic sensing patch with naked eyes or smartphone cameras. Additionally, the color difference observed from different viewing angles may also affect the accuracy of pH monitoring. To solve this issue, view angle-dependent holographic sensors remain an unmet need to improve accuracy, stability, and applicability. One possible strategy is that the shape of diffraction gratings needs to be changed to allow sensor interrogation from a broader range of viewing angles (Figure 1b). Although using retroreflectors as the recording object gave a broad viewing angle range of 25°–85°, the fabricated holographic sensors displayed a wavelength shift of over 85 nm in total at different viewing angles.[17] However, the fabricated holographic sensor displayed a wavelength shift of over 85 nm in total. In addition, the usage of high-order diffraction for viewing angle dependence optimization was used to broaden the viewing angle tolerance.[18] However, the complexity of the fabrication method using time-alternating switching of the fringe patterns and spatial filters hinders the large-scale production of holographic sensors.

Here, viewing angle-independent flexible holographic pH sensing films were fabricated using ball bearings as recording objects to quantify the wound pH variation reversibly and continuously during the inflammatory phase and early proliferation phase. Computational simulations of holographic pH sensor recording and readout processes for holograms fabricated using different reflective surfaces under UV laser exposure were first carried out to facilitate the viewing angle tolerance optimization. Experiments were carried out to validate simulation work results and characterize the performance of holographic sensors on the glass substrate. Then, the holographic sensing films can be integrated with commercial polyurethane (PU)-based wound dressings, making them a bandage to mount on users' skin and wound regions (Figure 1c). The flexible holographic pH sensing bandage with bending status was examined to simulate the mounting on skin surfaces. The reversibility and selectivity of flexible holographic pH sensors were tested in artificial wound exudate over a physiological range of pH values in chronic wounds. Continuous monitoring of pH value variations in the conformable holographic pH sensing bandages was carried out on a porcine skin model to validate its usage in POC settings.

2. Results and Discussion

2.1. Computational Simulation of Viewing Angle Tolerance Optimization

Holographic sensors are power-free and label-free sensing systems, which are embedded with the Bragg grating nanostructure and diffract narrow-band light according to Bragg's law. The inherently restricted viewing angle tolerance of holograms (<20°) of holographic sensors recorded using planar mirrors hinders the integration of holographic sensing with wearable devices.[12a] 3D computational models have been built to simulate the holographic recording and reading process based on solving electromagnetic wave equations in the complex field (Equation 1) in MATLAB R2021b via graphics process unit (GPU) processing.

$$\begin{cases} \mu\epsilon\frac{\partial^2 \mathbf{B}}{\partial t^2} + \mu\sigma\frac{\partial \mathbf{B}}{\partial t} - \nabla^2 B = 0 \\ \mu\epsilon\frac{\partial^2 \mathbf{E}}{\partial t^2} + \mu\sigma\frac{\partial \mathbf{E}}{\partial t} - \nabla^2 E = 0 \\ \epsilon + \frac{\sigma}{\omega}i = 8.85\times10^{-12}RI^2 \end{cases} \quad (1)$$

where μ is the permeability, ϵ is the permittivity, σ is the conductivity, ρ is the total electric charge density, ω is the angular frequency, B stands for the complex magnetic field, and E is the complex electric field. **Figure 2a** shows the schematics of the 3D computational model for the laser exposure step in hologram fabrication associated with the experimental laser interference method. The complex refractive index (RI) of the highly moisturized recording hydrogel and reflective surfaces were set to 1.34 and 1.9+2.4i, respectively, whereas the rest of the simulation space was designated as free space, which has an RI of 1. A boundary layer was designed to absorb light beyond the boundary (Figure S1, Supporting Information). A planar wave propagated across the recording hydrogel, reflected by various shapes of reflective surfaces and formed different interference patterns (Figure 2b). The light interference-induced antinodes have a higher intensity to initiate photopolymerization reactions of secondary monomer solution soaked in the primary hydrogel layer and form diffraction grating nanostructures with an RI set to 1.64 (Figure 2c).[16] Figure 2d illustrates the simulation of the holographic reading process, where a focal broadband light source was used as the incidence to obtain simulated diffraction

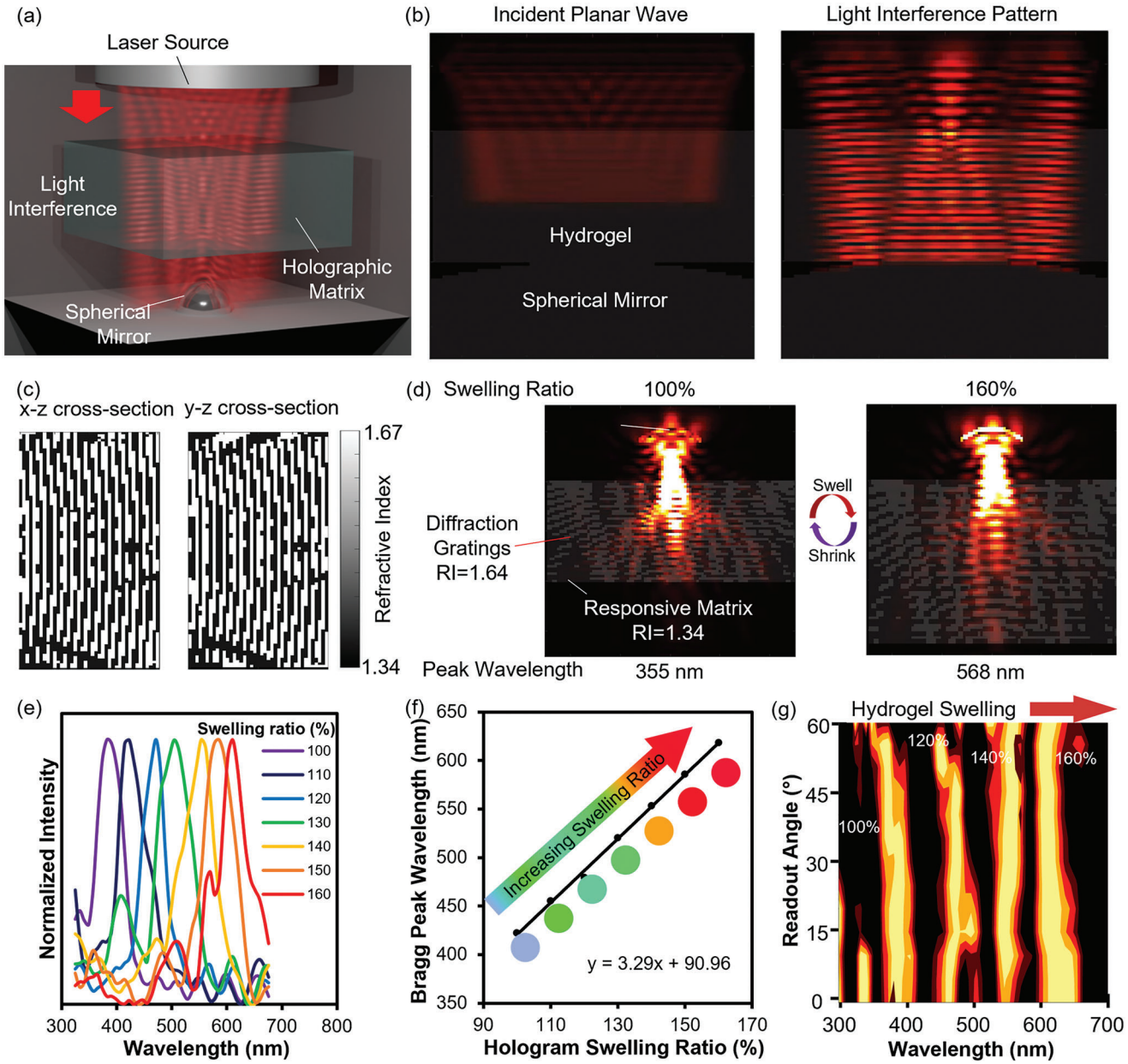

Figure 2. 3D simulation of holographic pH sensor recording and reading. a) 3D schematics of hologram recording simulations. b) Simulated light interference across the hydrogel. (c) Simulated diffraction gratings generated by laser interference. d) Simulated holographic reading at different swelling ratios of the holographic sensor. e) Simulated Bragg peak spectra of the holographic sensor at different hologram swelling ratios from 100% to 160%. f) The simulated calibration curve and color response of flexible holographic sensors. g) Simulated angle dependence contour plot at different swelling ratios.

spectra at different swelling ratios from 100% to 160% as the Bragg peak shifted from 422 nm to 618 nm. The simulation indicates that every 1% of hydrogel expansion results in a Bragg peak shift of 3.29 nm, experiencing a color change from blue to red in the visible spectra (Figure 2e,f). Different diameters of spherical mirrors (25 μm–5 mm) used in the laser exposure have also been simulated to investigate the effect of the size of spherical mirrors. The use of spherical mirror with diameters of 25 μm–5 mm under the single pulse exposure significantly broadened the viewing angle of holograms so that diffractive light peak can be detected from 0°–60° and a larger diameter generated stronger gratings and less wavelength shift at different viewing angles. However, due to the limit of computational power, the simulation with a larger diameter than 5 mm cannot be executed. The viewing angle tolerance was examined by taking diffraction spectra from different viewing angles, demonstrating around 60° of viewing angle range for ball-bearing holograms with a 195.9 nm wavelength shift in total at swelling ratios from 100% to 160% (Figure 2g). This simulation confirmed that using spherical mirrors to alter light interference patterns during laser exposure can

significantly optimize the viewing angle dependence of holographic sensors.

2.2. Fabrication of Viewing Angle-Independent Holographic pH Sensors

Theoretical simulation facilitated the experimental design of holographic pH sensors. Varying the convexity of the reflection surface under UV laser exposure is a viable way to broaden the viewing angle range of holographic sensors since it can change the shape of imprinted interference layers in the hydrogel (**Figure 3**a). The resulting diffraction gratings are spherical and reflect light into a broader angle range, as suggested by the theoretical simulation. Figure 3b illustrates the laser exposure setup with an Nd: YAG laser single-flash exposure (5 ns, 355 nm, 40 µs) and ball bearings as recording objects. The single flash incorporated diffraction gratings by initiating the highly crosslinked photopolymerization of the monomer solution (13 mol.% of hydroxyethyl methacrylate (HEMA), 82 mol.% of ethylene glycol dimethacrylate (EDMA), and 5 mol.% of 2-hydroxy-2-methylpropiophenone (HMPP)) in the obtained hydrogels from the first step polymerization of 70 mol.% of HEMA, 4 mol.% of EDMA, 1 mol.% of HMPP, and 25 mol.% of dimethylamino ethyl acrylate (DMAEA).[16] Characterizations of fabricated holographic pH sensors was carried out using a TRIS buffer solution (50 mmol L^{-1}) with a pH range of 6.25–9.00 at 37 °C in a water bath (Figure 3c). The sensor was illuminated by a broadband light source covering the whole visible light spectrum (Figure S2, Supporting Information), and the holographic sensing signal was then received by a bifurcated fiber optic and sent to a spectrophotometer and smartphone camera for quantitative and qualitative analysis, respectively. The illumination of holographic pH sensors with a broadband light source, which is safe for the skin, eliminated the need to remove wound dressings from the wound for the readout. The angle dependence measurement was accurately controlled using a goniometer. As the pH value decreases, the holographic pH sensor swells, resulting in a red shift in the diffraction light (Figure 3d). Figure 3e,f demonstrated the Bragg peak spectra and calibration curve obtained by the spectrophotometer in a TRIS buffer solution with a pH range of 6.25–9.00. The inset figure illustrates the smartphone camera captured photographs of holographic sensors. Holographic pH sensors demonstrated a significant Bragg wavelength shift over 270 nm in this pH range, where the holographic pH sensor yielded a 143 nm shift per pH unit in the physiological range of chronic wound pH (7.15–8.50). The calibration curve shows similar sensitivity and replay wavelength to planar-mirror holographic pH sensors (Figure S3a,b, Supporting Information). The size of the ball bearing under the laser exposure is of great significance since it directly affects the geometry of imprinted interference layers in hydrogels. At the infinitesimal area where the hydrogel touches the spherical surface, a more miniature ball bearing deviates more from the planar mirror, leading to a broader interrogation angle range but also a more significant wavelength difference (50 nm) at different interrogation angles and a smaller readout area (Figure S4, Supporting Information). When using the ball bearing size of 35 mm diameter, the viewing angle range was expanded to over 35°. Compared to a holographic pH sensor recorded using a planar mirror of which the viewing angle range is less than 15°, the viewing angle dependence has been relaxed significantly (Figure S3c, Supporting Information). Figure 3g(i) demonstrates the replay wavelength remains consistent at different viewing angles from 15°–45° at pH 8.00, which ensures an accurate sensor interrogation regardless of the viewing angle of the hologram. However, a noticeable replay wavelength difference from different viewing angles was observed when the hologram expanded at a lower pH value in the TRIS buffer solution (Figure 3g(ii)). The viewing angle tolerance was significantly improved to 37° at pH 8.50 and became broader at a lower pH value (Figure 3h). The replay wavelength is directly related to the grating spacing based on Bragg's law (Equation 2)

$$n\,\lambda_{peak} = 2dsin\,(\theta) \tag{2}$$

where λ_{peak} is the peak wavelength of the diffractive light and d is the grating spacing. At lower pH, since the rigidity of the glass substrate is restricting holograms from expanding along the substrate, the expansion of holograms in the normal direction stretched the grating into a non-spherical shape, where the observed grating spacing at a larger viewing angle is smaller than that observed at a lower viewing angle. The wavelength shift can be reduced when holographic pH sensors are integrated with stretchable substrates that allow holograms to expand in all three directions so that the grating nanostructure can maintain its concentric spherical shape. However, hydrogel expansion in other dimensions may reduce the sensitivity of holographic pH sensors.[19]

2.3. Fabrication and Characterizations of Flexible Holographic pH Sensors

To construct a wearable analytical device, holographic sensors need to be integrated on flexible substrates instead of rigid glass slides. The choice of substrates must meet the criteria that it should not affect the optical properties of diffractive light. Therefore, they cannot be optically active or birefringent.[12a] Polyurethane (PU) substrates have been used as commercial wound dressings for their ultimate flexibility and biocompatibility. The transparency of the film and the adhesiveness of the additional acrylate layer also make them ideal platforms for integrating hydrogel-based holographic sensors. A thin layer of poly(HEMA) hydrogel was fabricated on an ultra-thin untreated glass slide and then transferred onto the PU substrate by detaching the hologram from the glass slide using a 50% (v/v) methanol-water solution (**Figure 4**a). The interrogation optical setup was demonstrated in Figure 4b, where curved surfaces were used to simulate the curvature of skin surfaces. The flexible holographic sensor was first characterized in the TRIS buffer solution on a flat surface as a control group. The flexible holographic pH sensors have a wavelength shift of 131 nm from pH 6.50 to 8.75, while the rigid holographic sensors showed a shift of 267 nm from pH 6.50 to 8.75 (Figure 4c,d). This shift reduction might be caused by the expansion of holograms to other dimensions due to the stretchability of PU substrates, while it will not affect the interrogation since the holographic sensor still demonstrated significant color changes in the visible spectra. Since the

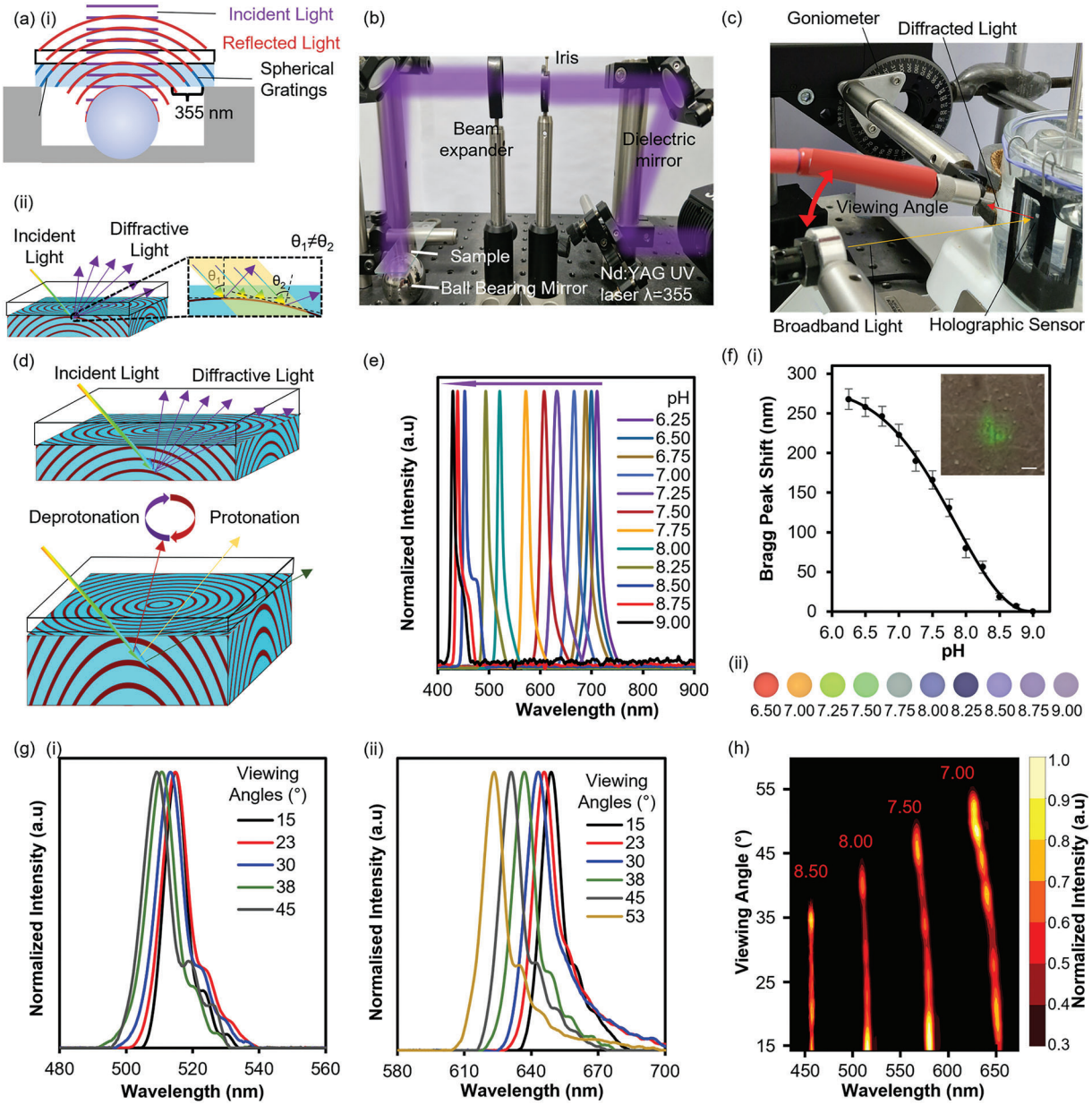

Figure 3. Optimization of viewing angle tolerance of holographic pH sensors using ball bearings as the recording surface under UV laser exposure. a) (i) Schematic of the recording process of holographic pH sensor using a ball bearing as the recording object. (ii) Schematic of the interrogation of holographic sensors with spherical gratings. The spherical gratings allow light to be diffracted in different directions. b) Photograph of the optical setup of the Nd: YAG laser exposure. c) Photograph of the in vitro optical setup for holographic sensor readout and viewing angle tolerance measurement. d) Schematic of broadening the viewing angle of holographic sensors by altering the shape of imprinted interference layers with hydrogels at an unswollen state. The replay wavelength differences from different viewing angles were caused by the one-directional expansion of holograms restricted by rigid glass substrates. e) Normalized diffraction spectra of ball-bearing holographic pH sensor collected throughout the TRIS buffer solution measurements in cuvettes. f) i, Calibration curve of Bragg peak shift in TRIS buffer solutions from pH of 6.25 to 9.00, where error bars represent calculated standard error based on twenty independent readings (n = 20). The inset figure shows a ball-bearing holographic pH sensor (scale bar = 500 μm). ii, Colourimetric response of the holographic pH sensor. (g) Bragg peak shift at different viewing angles at a pH of i, 8.00 and ii, 7.00 in the TRIS buffer solution. (h) Viewing angle tolerance measurements of ball-bearing holographic pH sensors.

working principle of holographic sensors is based on the imprinted diffraction grating nanostructure, mechanical manipulations, such as bending or wrinkles, might affect the accuracy of the readout. The holographic pH sensor mounted on curved surfaces with a diameter larger than 30 mm only gave ≈5 nm replay wavelength difference in the TRIS buffer solution with a pH of 6.50 (Figure 4e). Figure 4f demonstrated that bending the flexible holographic pH sensor did not influence the normal readout when mounted on cylindrical surfaces with a diameter above 30 mm for readout in a TRIS buffer solution of a pH

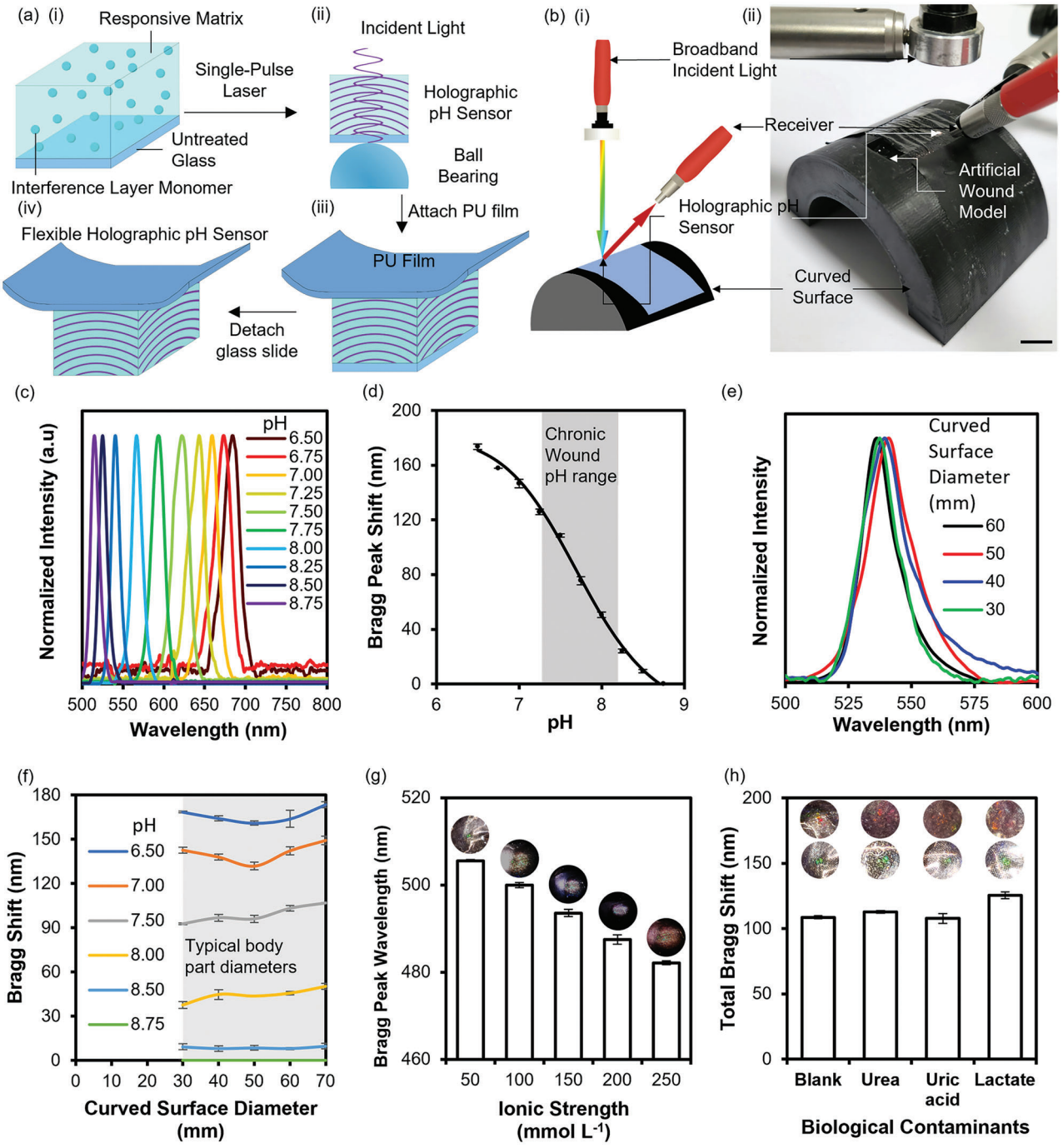

Figure 4. Commercial polyurethane wound dressing can be used as the substrate of holographic sensors. a) The fabrication process of a flexible holographic pH sensor on the PU substrate for wound healing monitoring i, Diffusion of interference layer monomers into the responsive matrix temporarily attached to an untreated ultra-thin glass slide. ii, Exposure of the hydrogel over a ball bearing with the hydrogel side facing upward. iii, Attach the exposed holographic pH sensor onto commercial PU substrates via an adhesive layer. iv, Detachment of the glass slide. b) i, Schematic of flexible hologram readout on the curved surfaces to characterize the effect of bending on the readout of holographic pH sensor mounted on skin. ii, The photograph of the setup (scale bar = 10 mm). c) Normalized flat flexible holographic pH sensor spectra were collected throughout TRIS buffer solution measurements. d) The calibration curve of Bragg peak shift in TRIS buffer solutions from pH of 6.25 to 9.00, where error bars represent the standard error of nine independent readings (n = 9). e) Normalized Bragg peak spectra for flexible holograms of different bending diameters at a pH of 6.50. f) The effect of bending on the normalized Bragg reflection spectra at pH 9 and 6.50, where error bars represent the calculated standard error of twelve independent reading (n = 12). g) Bragg peak wavelength taken from holographic sensors in a TRIS buffer solution of a concentration of 50 mmol L^{-1} and pH of 7.00 with an ionic strength range of 50–250 mmol L^{-1}, where error bars represent calculated standard error of twelve independent reading (n = 12). h) Bragg peak shift of holographic sensors tests in AWE from pH of 7.00 to 8.00 with the presence of urea, uric acid, and lactate at a concentration of 8.90, 0.35, and 10.90 mmol L^{-1}, respectively. Error bars represent the calculated standard error of three independent readings (n = 3).

range of 6.50–8.75. The use of ball bearing in the holographic recording process generated spherical shape interference layers, which eliminated the effect of wrinkles when wearing the bandage (Figure S5, Supporting Information). The stability of holographic sensor readout under bending status allows for accurate pH quantification in wound exudates when they are mounted on body surfaces.

The sensing performance of the holographic pH sensor might be affected by ionic strength variations in the target fluid since the working principle relies on the osmotic and electrostatic force-driven volumetric change of the hydrogel.[16] Figure 4g demonstrated normalized spectra of flexible holographic pH sensor testing in TRIS buffer solutions of pH 7.00 with an ionic strength range of 50–250 mmol L^{-1}. A total Bragg peak shift of ≈22 nm was observed, where higher ionic strength led to less Bragg peak shift due to the reduction of osmotic pressure difference and electrostatic force exerted on the holographic pH sensor. Nevertheless, the physiological variations of ionic strength in wound exudate are not significant to affect the readout of flexible holographic wound pH sensors.[16,20] The selectivity of the fabricated flexible holographic pH sensor was then tested in the TRIS buffer solution in the presence of other common electrolytes and metabolic excrement in the wound milieu. The physiological concentrations of urea (8.9 mmol L^{-1}), uric acid (347 µmol L^{-1}), and sodium lactate (10.9 mmol L^{-1}) were introduced to the TRIS buffer solution at pH of 7.50 and 8.75. The Bragg peak shifts shown by holographic pH sensors were similar, with minimal impact from biological contamination (Figure 4h). This indicated a high selectivity of holographic pH sensors towards the pH value of the analyte solution with the presence of common biological contaminants since the polymerized form of HEMA, EDMA, and DMAEA are unable to interact with the physiological concentration of urea, urate, and lactate ions, and thereby unable to stimulate the volumetric response of the hydrogel.

2.4. Wound Monitoring in an Ex Vivo Skin Model

A conformable pH sensing bandage was fabricated as a wearable wound care dressing by incorporating the flexible PU-based holographic pH sensor with a black cotton layer. A breathable backing layer can be added to the back side of the holographic pH sensor. From the square observation window (6 × 6 mm) on the breathable backing layer, the colorimetric response of holographic pH sensors can be read by the naked eye or a smartphone camera (**Figure 5**a(i)). Figure 5a(ii) demonstrates the side view of the holographic sensing bandage design. The black cotton layer acts as a dark background to reduce the noisy white scattering from the skin surface and an absorption layer to facilitate the transport of wound exudate toward the holographic pH sensor. The bandage showed a clear red shift as the pH value increased, allowing the qualitative analysis of wound milieu pH via the naked eye. The sensing bandage was then tested on an artificial wound model on an ex vivo porcine skin model. A distinguishable color replay could be observed from holographic pH sensors mounted on the porcine skin model from different viewing angles (Figure 5b). The holographic sensing signal remained visible when the smartphone camera was taking photographs at different viewing angles (Movie S3, Supporting Information). The holographic sensing bandage underwent a color change from red to green in the pH range of 7.00–8.75. However, due to the change in ionic strength, the holographic pH sensing requires calibration in AWE. To stabilize the pH value of AWE, 50 mmol L^{-1} TRIS was added to AWE. Figure 5c demonstrates the Bragg diffraction spectra of holographic pH sensing bandage in AWE with a pH range of 7.00–8.75 in increments of 0.25 taken using a spectrophotometer. Calibration curves of holographic pH sensing bandage in the TRIS buffer solution and AWE provided similar sensitivity to pH variations, validating the applicability in biological analytes (Figure 5d). The linear relationship allows for accurate colorimetric quantification of pH value over the 7.00–8.75. The reversibility of the holographic pH sensor provides a chance for continuous and real-time monitoring of the pH value of the wound exudate. To test the ability of continuous and real-time monitoring, the sensor was repeatedly used to detect AWE of pH of 7.00 and 8.75 (Figure 5e). The sensor exhibits minimal variations in the Bragg peak wavelength at both low and high pH values, indicating a reversible binding between hydrogen ions and DMAEA in the hydrogel and reliability in the presence of contaminants. This ensures an accurate and continuous quantification of pH value in wound exudate without signal drift and recalibration requirements in long-term usage.

AWE with a pH range of 7.00 to 8.75 was pipetted into the artificial wound model to simulate the variation of pH value during the wound healing process. A black cotton bud was attached to the hydrogel surface to reduce the white scattering from the pale-colored skin, and thereby improve the signal-to-noise ratio (SNR). The porous and soft structure and excellent biocompatibility of cotton buds also facilitate the transport of AWE to the hydrogel and better wearability for ultrasensitive wound areas. Figure 5f,g demonstrates the ability of holographic pH sensing bandages to continuously monitor pH variations in AWE in an artificial wound model. The flexible holographic pH sensing bandage shows a quick response to pH variations with minimal deviations in each measurement within 540 min of continual usage. The continuous movement, bending, and twisting have minimal impact on the holographic signal (Movie S4, Supporting Information). Figure S6 (Supporting Information) shows that the holographic pH sensing bandage posed minimal color change under continuous mechanical manipulations, which proved the stability of reading when mounted on human skin. The integration of holographic pH sensors and PU film substrates provides a flexible, cheap, accurate, and reliable wound pH sensing platform at POC settings, which supports colorimetric readout and continuous pH monitoring. The colorimetric response can be detected by CMOS sensors embedded in smartphone cameras as the color change gave a significant Hue value change in captured photographs in response to the pH variation in the wound milieu (Figure 5h). The hue value varied by 120 from the pH of 8.75 to 7.00. This allows the use of smartphone cameras for the sensor readout with either photograph taken prior or at the moment since the wavelength information is converted to the hue value that can be recognized by the smartphone. Since pH is closely related to the wound healing process, continuous monitoring offers a chance to have a deeper insight and give timely warning and necessary medical treatment accordingly.

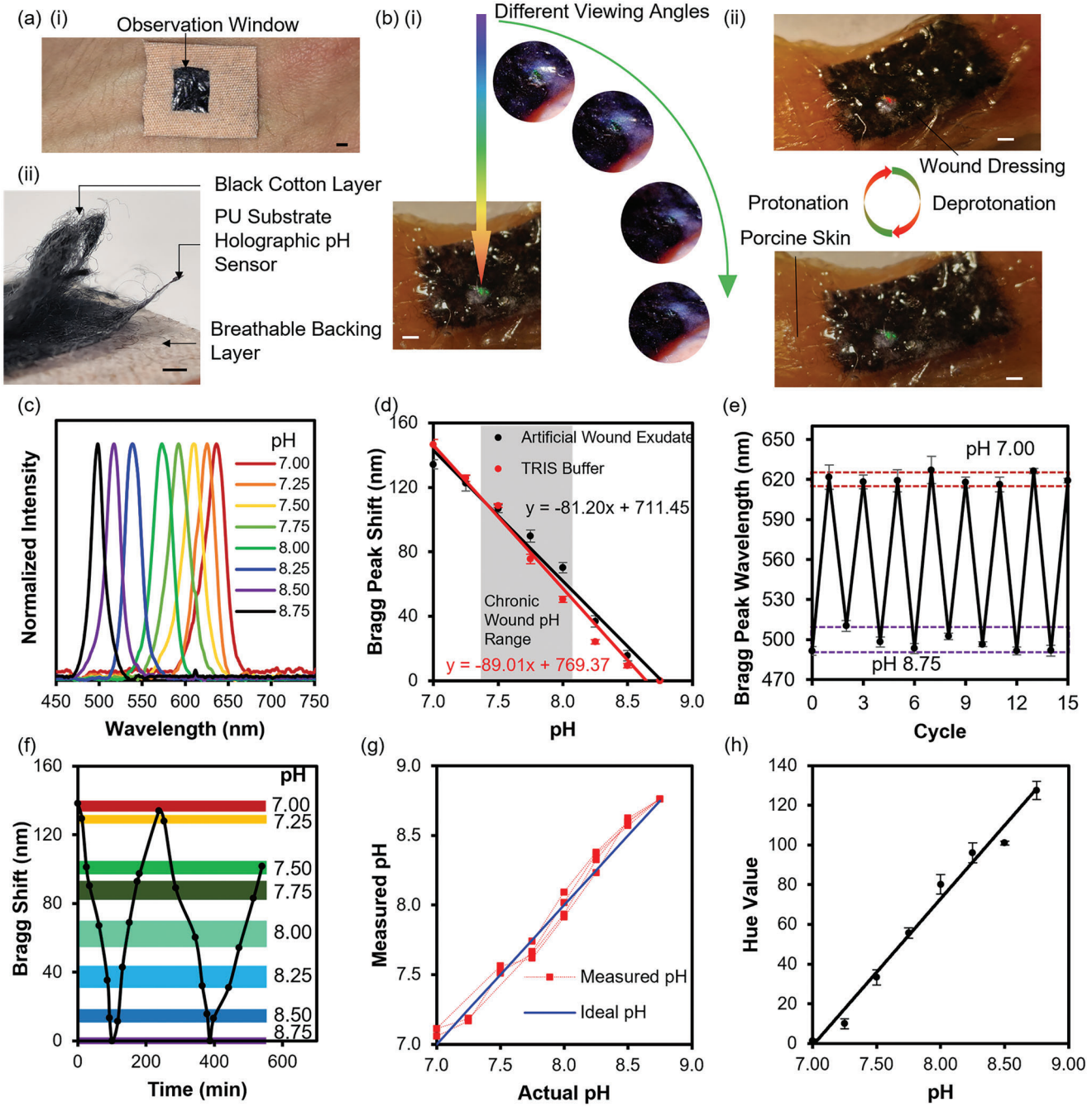

Figure 5. Characterizations of conformable holographic pH sensing bandage in AWE and porcine skin model. a) The photograph of the fabricated wound pH sensing bandage (scale bar = 2 mm). i, Photographs of the front view of the sensing bandage mounted on human skin and the colorimetric response observed from the observation window. ii, Photographs of the peel-off structure of the conformable holographic pH sensing bandage. b) i, Photographs of the holographic sensing bandage taken by the smartphone camera from different viewing angles. The holographic signal remained visible until the photograph was taken at a large viewing angle. ii, Smartphone camera captured photographs of a holographic pH sensing bandage on an ex vivo porcine skin model demonstrating colorimetric response to pH variations in AWE (scale bar = 2 mm). c) Normalized Bragg peak of flexible holographic pH sensors tested in AWE with a pH range of 7.00–8.75. d) Comparison of the conformable holographic pH sensing bandage calibration curves in a TRIS buffer solution and AWE, where error bars represent the calculated standard error of nine independent readings (n = 9). e) Test of reversibility of conformable holographic sensing bandage in AWE between pH of 7.00 and 8.00, where error bars represent standard errors of three independent readings (n = 3). f) Continuous monitoring of pH variations in AWE on porcine skin model, where error bars represent standard errors of three independent readings (n = 3). g) Comparison between the actual pH value of AWE and measured pH value read from the holographic pH sensing bandage on the porcine skin model. h) The hue value extracted from smartphone-captured photographs of the conformable holographic pH sensing bandage in response to the pH variation in AWE, where error bars represent the calculated standard error of three independent readings (n = 3).

3. Conclusion

In this work, a conformable holographic pH sensing bandage was fabricated using a commercialized PU wound dressing substrate with a more relaxed viewing angle tolerance. The viewing angle tolerance was optimized via hologram recording using ball-bearing mirrors, improving the applicability in wearable devices for daily wound healing monitoring. Computational simulation of hologram recording and reading at different swelling ratios facilitated viewing angle tolerance optimization study. Integrating PU film as a substrate allows excellent flexibility of the holographic pH sensing bandage. The conformable holographic pH sensing bandage can determine the pH value in wound exudate with a pH range of 7.00–8.75, with a colorimetric response that can be interrogated quantitatively and qualitatively. The total Bragg peak shift of the holographic pH sensing bandage is approximately 134.7 nm with a viewing angle range of 15–53° away from the incident light. The bandage was also tested in AWE in the presence of common electrolytes and biological contaminants, demonstrating their selectivity, reliability, and reversibility. The design of the bandage included a dark-colored absorbent cotton layer, a sensing layer, and a breathable backing layer. The conformable wound pH sensing bandage based on holographic sensing principles demonstrated good ability in continual monitoring of wound pH variations on an ex vivo porcine skin model. The colorimetric response allows POC interrogation of sensors via naked eyes and smartphone cameras. However, wound healing monitoring accuracy needs to be improved by monitoring multiple biomarkers (e.g., calcium ion, magnesium ion, matrix metalloproteinases, and interleukins) simultaneously, and this could be achieved by miniaturizing multiple holographic sensors such as glucose sensors.[15] The development of a holographic sensor readout smartphone application also provides a means for quick data acquisition from the holographic wound sensor. A smartphone-based portable spectrophotometer can be developed for higher accessibility of the holographic sensing bandage to offer a strategy for accurate and timely wound assessment in POC settings, thus, reducing socio-economic burdens on the National Health Service.[21]

4. Experimental Section

Materials: All chemicals were analytical grade. 3-(trimethoxy silyl)-propyl methacrylate, acetone, hydroxy ethyl methyl methacrylate (HEMA), ethylene glycol dimethacrylate (EDMA), 2-(dimethyl amino) ethyl acrylate (DMAEA), 2-hydroxy-2-methylpropiophenone (HMPP), isopropanol, tris(hydroxymethyl)amino methane (TRIS), TRIS hydrochloride (TRIS HCl), potassium chloride, calcium chloride, magnesium chloride, sodium bicarbonate, urea, uric acid, sodium lactate, and hydrochloric acid (1 mol L^{-1}) were purchased from Sigma Aldrich. Methanol, glucose, and sodium chloride were purchased from VWR. Aluminized polyester films were purchased from HiFi Industrial Film Ltd., commercialised PU wound dressings were purchased from Abeillo, cotton layers were purchased from Synergy Health (UK) Ltd.

Equipment: Microscope slides were purchased from Fisher Scientific, cover glass slides from VWR, and the UVP crosslinker from Analytik Jena. Nd: YAG frequency tripled Quantel Q-smart (5 ns, 355 nm) solid-state laser purchased from Lumibird, France. The drying oven UN30 used for hydrogel drying was purchased from Memmert. The plano-concave lens (−75.0 mm, Ø1″ UV fused silica plano-concave lens, uncoated), optical posts (Ø12.7 mm, L = 20 mm), pedestal post holder (L = 20 mm, Ø12.7 mm), power and energy meter interface (PM100USB), UV extended Si photodiode, motorized precision rotation stage (Ø1″), collimated laser-diode-dumped DPSS laser module (532 nm, 4.5 mW), laser diode module mounting Kit (Ø11 mm), and iris (mounted standard iris, Ø12 mm max aperture, TR3 Post) were purchased from Thorlabs, United States. A 25 mm dielectric 355 nm Nd: YAG laser line mirror was purchased from Edmund Optics, UK. Fisherbrand classic vortex mixer was purchased from Fisher Scientific, Bishop Meadow, UK. The Mettler Toledo FiveEasy Plus pH benchtop meter was purchased from Mettler-Toledo Ltd. Orion Star A212 Benchtop Conductivity Meter from ThermoFisher. Holographic responses were analyzed using UV-vis bifurcated fiber optical cables, a 20 W tungsten halogen broadband light source, Flame-S-VIS-NIR-ES spectrophotometer, and Oceanview software (2.0.8) purchased from Ocean Insight. Ball bearings used as hologram recording objects were purchased from Simply Bearings Ltd.

Holographic Sensor Fabrication and Readout Simulation: The simulation includes two sections: hologram fabrication and sensor reading. In the fabrication simulation, a planar light source with a wavelength of 355 nm was used. A three-dimensional matrix of 100 × 100 × 100 with a resolution of 50 nm was set for simulation with an absorbing boundary layer with a width of 10 pixels.[22] The permeability μ was assumed to be constant at $1.25663753 \times 10^{-6}$ H m^{-1} through the whole matrix. The permittivity ϵ was defined in the each pixel based on the refractive index n of free space and hydrogel based on the equation $n = \sqrt{\frac{\epsilon_r}{\epsilon_0} \times \frac{\mu_r}{\mu_0}}$. The tilted angle of the hydrogel and the shape of the mirror were varied in the simulation to find the best experimental configurations for hologram fabrication. The exposure intensity of hydrogel at each pixel was calculated and results in the change of refractive index of specific pixels at antinodes of the light interference. The resulting hydrogel matrix was then passed to the sensor reading simulation. In the sensor reading simulation, the fabrication simulation output matrix was used. A convex light source was used to simulate the reading process. The intensities of the incident and reflected beams were measured at different reading angles. Experiments will validate the simulated results.

Fabrication of Holographic Sensors: All procedures were carried out in light-tight conditions unless mentioned otherwise. Microscope slides were silanized using a solution of 3-(trimethoxysilyl) propyl methacrylate in acetone at a ratio of 1:50 (v/v) overnight. Silanized glass slides were then washed using methanol and stored in light-tight conditions. The primary monomer solution was prepared using HEMA (70 mol.%), EDMA (4 mol.%), HMPP (1 mol.%), and DMAEA (25 mol.%) in brown bottles. The primary solution was then diluted using propan-2-ol at a ratio of 1:1. The secondary monomer solution was prepared using HEMA (13 mol.%), EDMA (82 mol.%), and HMPP (5 mol.%). The solution was then diluted with 90% methanol solution at a ratio of 1:1. On the polyester side of a flat aluminized polyester film, 50 μL of the primary monomer solution was pipetted, and a silanized glass slide was placed onto the droplet. It was then exposed under 4 UV (A) strip lights for 30 min. The polymerized primary hydrogel layer was then removed from the polyester film and washed in methanol in water at a ratio of 1:1 (v/v) for 30 min to remove any by-products and unpolymerized monomers from the hydrogel layer. The hydrogel was then wiped dry, and 150 μL of the secondary monomer solution was pipetted onto a clean, flat, aluminized polyester film. Hydrogel side facing downward, the slide was then placed on the droplet to allow the hydrogel to be soaked in the secondary monomer solution for 5 min. The hydrogel surface was then given a single wipe to remove excessive secondary monomer solution. The hydrogel was then dried in an oven at 55 °C for 5 min. The hydrogel was then left to cool down to 25 °C. Since the thickness of hydrogel at laser exposure was a critical factor affecting replay wavelengths of holographic sensors, these steps must be maintained at the same temperature and humidity. The slide was then placed on the top of a planar mirror with a tilted angle of 5° to separate the diffraction light from the incident light. Slides were then exposed to a single flash of an Nd: YAG laser (5 ns, 355 nm, 40 μs delay). The exposed holograms were then washed using 50 vol.% methanol solution

overnight to remove excessive monomers and any by-products during the photopolymerization.

Optimization of Viewing Angle Tolerance: Instead of placing the slide on a planar mirror, the slide was then placed on the top of the ball bearing with a diameter of 35 mm. The hydrogel was held horizontally. Slides were then exposed to a single flash of Nd:YAG laser (5 ns, 355 nm, 40 µs delay). The exposed holograms were then washed using 50 vol.% methanol solution overnight to remove excessive monomers and any by-products during the photopolymerization.

Flexible Holographic pH Sensing Bandage Fabrication: Instead of silanized glass slides, the primary hydrogel layer was prepared on an ultrathin clean, untreated cover glass slide to transfer the film onto flexible substrates after the laser exposure. To maintain the flatness of hydrogel, the hydrogel can be sandwiched with another clean glass slide during the first washing step. During the laser exposure, the glass slide side was facing downward instead to maintain the exact orientation of imprinted nanograting. After the laser exposure, an adhesive polyurethane film was attached to the hydrogel and then submerged in methanol-water solution (1:1 v/v) overnight to remove unpolymerized monomers and detach holograms from the cover glass.

Characterizations of Flexible Holographic pH Sensor: The flexible holographic sensor was cut using a scalpel and fixed on the top of artificial wound models with the hydrogel side facing the solution. Buffer solutions were prepared in a pH range of 6.25–9.00 using Tris(hydroxymethyl)aminomethane (TRIS), TRIS Hydrochloride, and potassium chloride at a constant concentration of 50 mmol L^{-1} and ionic strength of 50 mmol L^{-1}. The pH value can be corrected using 1 mol L^{-1} hydrochloric acid and confirmed by the Mettler Toledo FiveEasy Plus pH benchtop meter. Buffer solutions were added to the artificial wound model to characterize flexible holographic pH sensors. A broadband light source was used to illuminate the holographic pH sensor, and the diffractive light was detected using bifurcated optical fibers and sent to an Oceanview Flame spectrophotometer. The reading of the Bragg peak wavelength needs to be taken when the peak was at equilibrium. The artificial wound model needs to be rinsed three times with buffer solution among each measurement of different pH values. By varying the diameter of the curved surface, the effect of bending on holographic pH sensor interrogation can be tested.

Fabrication of Holographic pH Sensing Wound Dressing: All procedures were carried out in light-tight conditions unless mentioned otherwise. Using the same formulation of primary and secondary monomer solutions. On the polyester side of a flat aluminized polyester film, 31 µL of the primary monomer solution was pipetted, and a clean ultrathin glass slide was placed onto the droplet. It was then exposed under 4 UV (A) strip lights for 30 minutes. The polymerized primary hydrogel layer was then removed from the polyester film and washed in methanol in water at a ratio of 1:1 (v/v) for 30 min to remove any by-products and unpolymerized monomers from the hydrogel layer. During the methanol wash, the hydrogel was sandwiched to remain the attachment between the hydrogel and the clean glass slide. The hydrogel was then wiped dry, and 150 µL of the secondary monomer solution was pipetted onto a clean, flat, aluminized polyester film. The hydrogel side facing downward, the slide was then placed on the droplet to allow the hydrogel to be soaked in the secondary monomer solution for 5 min. The hydrogel surface was then given a single wipe to remove excessive secondary monomer solution. The hydrogel was then dried in an oven at 55 °C for 5 min. The hydrogel was then left to cool down to 25 °C. Since the thickness of hydrogel at laser exposure was a critical factor affecting replay wavelengths of holographic sensors, these steps must be maintained at the same temperature and humidity. The slide was then placed on the top of a ball bearing horizontally. Slides were then exposed to a single flash of Nd: YAG laser (5 ns, 355 nm, 40 µs delay). The exposed holograms were then attached to the PU film using the adhesive layer. The whole slides were then washed using 50 vol.% methanol solution overnight to remove excessive monomers and any by-products during the photopolymerization. As the hydrogel swells in the methanol solution, the detachment of the hydrogel from the glass slide will take place, thereby a holographic pH sensing bandage can be obtained.

Artificial Wound Exudate (AWE) Formulation and Ex Vivo Test: AWE solution contains physiological concentrations of common electrolytes and biological contaminants. The AWE was prepared by dissolving sodium chloride (128.83 mmol L^{-1}), magnesium chloride (0.94 mmol L^{-1}), calcium chloride (2.23 mmol L^{-1}), sodium bicarbonate (19.00 mmol L^{-1}), glucose (1.80 mmol L^{-1}), albumin (22 g L^{-1}), potassium chloride (4.40 mmol L^{-1}), urea (8.90 mmol L^{-1}), uric acid (0.35 mmol L^{-1}), and sodium lactate (10.90 mmol L^{-1}) in deionized water. To stabilize the pH of AWE, TRIS and TRIS HCl were added to the AWE solution by maintaining TRIS concentration at 50 mmol L^{-1} and a pH range of 7.00–8.75. The pH value of AWE solutions was corrected using a small amount of 1 mol L^{-1} hydrochloric acid and confirmed using the pH meter. Continuous monitoring was achieved using AWE solutions on the porcine skin model. On each change of pH value, the artificial wound model was rinsed using an AWE solution three times to ensure a reliable pH in the artificial wound model for holographic pH sensor interrogation.

Statistical Analysis: Spectra taken by the spectrophotometer were firstly processed by the Savitzky–Golay filter and then subtracted by broadband light spectra taken before the measurement. The processed spectra were then normalized to [0,1]. All replay wavelength and Bragg peak shift data were expressed as mean ± standard error. All the abovementioned data processing was carried out using Origin 2020. The overlay contour plots for angle dependence measurements were processed by subtracting previously taken broadband light spectra and then normalized to [0,1]. The data processing was carried out using Python 3.9.7 with Matplotlib and NumPy libraries.

Supporting Information

Supporting Information is available from the Wiley Online Library or from the author.

Acknowledgements

A.K.Y. and Y.H. acknowledge Engineering and Physical Sciences Research Council (EPSRC) (NO. EP/T013567/1). N.J. acknowledges the National Natural Science Foundation of China (no. 82102182), the Fundamental Research Funds for the Central Universities (no. YJ202152), and JinFeng Laboratory, Chongqing, China (jfkyjf202203001). Y.M. thanks the European Union's Horizon 2020 research and innovation programme under the Marie Sklodowska-Curie grant agreement No 896410.

Conflict of Interest

The authors declare no conflicts of interest.

Data Availability Statement

The data that support the findings of this study are available from the corresponding author upon reasonable request.

Keywords

double photopolymerization, holographic sensors, viewing angle tolerance, wearable sensing bandages, wound healing monitoring

Received: July 21, 2023
Revised: December 13, 2023
Published online: January 7, 2024

[1] S. Guo, L. A. Dipietro, *J. Dent. Res.* **2010**, *89*, 219.
[2] a) X. Xiao, X. Xiao, A. Nashalian, A. Libanori, Y. Fang, X. Li, J. Chen, *Adv. Healthcare Mater.* **2021**, *10*, 2100975; b) C. K. Sen, G. M. Gordillo, S. Roy, R. Kirsner, L. Lambert, T. K. Hunt, F. Gottrup, G. C. Gurtner, M. T. Longaker, *Wound Repair Regen* **2009**, *17*, 763.
[3] a) T. Velnar, T. Bailey, V. Smrkolj, *J. Int. Med. Res.* **2009**, *37*, 1528; b) P. Mostafalu, A. Tamayol, R. Rahimi, M. Ochoa, A. Khalilpour, G. Kiaee, I. K. Yazdi, S. Bagherifard, M. R. Dokmeci, B. Ziaie, S. R. Sonkusale, A. Khademhosseini, *Small* **2018**, *14*, 1703509.
[4] M. S. Brown, B. Ashley, A. Koh, *Front. Bioeng. Biotechnol.* **2018**, *6*, 47.
[5] a) Y. Gao, D. T. Nguyen, T. Yeo, S. B. Lim, W. X. Tan, L. E. Madden, L. Jin, J. Y. K. Long, F. A. B. Aloweni, Y. J. A. Liew, M. L. L. Tan, S. Y. Ang, S. D./.O. Maniya, I. Abdelwahab, K. P. Loh, C.-H. Chen, D. L. Becker, D. Leavesley, J. S. Ho, C. T. Lim, *Sci. Adv.* **2021**, *7*, eabg9614; b) T. Guinovart, G. Valdés-Ramírez, J. R. Windmiller, F. J. Andrade, J. Wang, *Electroanalysis* **2014**, *26*, 1345; c) R. Rahimi, M. Ochoa, T. Parupudi, X. Zhao, I. K. Yazdi, M. R. Dokmeci, A. Tamayol, A. Khademhosseini, B. Ziaie, *Sens. Actuators B* **2016**, *229*, 609; d) V. Sridhar, K. Takahata, *Sens. Actuators A* **2009**, *155*, 58.
[6] a) C. Gamerith, D. Luschnig, A. Ortner, N. Pietrzik, J.-H. Guse, M. Burnet, M. Haalboom, J. Van Der Palen, A. Heinzle, E. Sigl, G. M. Gübitz, *Sens. Actuators B* **2019**, *301*, 126966; b) B. Greener, A. A. Hughes, N. P. Bannister, J. Douglass, *J Wound Care* **2005**, *14*, 59.
[7] B. Dalisson, J. Barralet, *Adv. Healthcare Mater.* **2019**, *8*, 1900764.
[8] M. Qin, H. Guo, Z. Dai, X. Yan, X. Ning, *J Semicond* **2019**, *40*, 111607.
[9] A. Pal, D. Goswami, H. E. Cuellar, B. Castro, S. Kuang, R. V. Martinez, *Biosens. Bioelectron.* **2018**, *117*, 696.
[10] a) G. J. Mohr, H. Müller, B. Bussemer, A. Stark, T. Carofiglio, S. Trupp, R. Heuermann, T. Henkel, D. Escudero, L. González, *Anal. Bioanal. Chem.* **2008**, *392*, 1411; b) Y. Zhu, J. Zhang, J. Song, J. Yang, Z. Du, W. Zhao, H. Guo, C. Wen, Q. Li, X. Sui, L. Zhang, *Adv. Funct. Mater.* **2020**, *30*, 1905493.
[11] G. Panzarasa, A. Osypova, C. Toncelli, M. T. Buhmann, M. Rottmar, Q. Ren, K. Maniura-Weber, R. M. Rossi, L. F. Boesel, *Sens. Actuators B* **2017**, *249*, 156.
[12] a) A. K. Yetisen, I. Naydenova, F. Da Cruz Vasconcellos, J. Blyth, C. R. Lowe, *Chem. Rev.* **2014**, *114*, 10654; b) S. Davies, Y. Hu, N. Jiang, J. Blyth, M. Kaminska, Y. Liu, A. K. Yetisen, *Adv. Funct. Mater.* **2021**, *31*, 2105645; c) N. Jiang, S. Davies, Y. Jiao, J. Blyth, H. Butt, Y. Montelongo, A. K. Yetisen, *ACS Sens.* **2021**, *6*, 915; d) S. Kabilan, A. J. Marshall, F. K. Sartain, M.-C. Lee, A. Hussain, X. Yang, J. Blyth, N. Karangu, K. James, J. Zeng, D. Smith, A. Domschke, C. R. Lowe, *Biosens. Bioelectron.* **2005**, *20*, 1602; e) I. Naydenova, P.-A. Blanche, *Elsevier* **2020**, *1*, 165; f) A. J. Marshall, J. Blyth, C. A. B. Davidson, C. R. Lowe, *Anal. Chem.* **2003**, *75*, 4423.
[13] a) E. Leite, I. Naydenova, S. Mintova, L. Leclercq, V. Toal, *Appl. Opt.* **2010**, *49*, 3652; b) M. Irfan, S. Martin, M. A. Obeidi, S. Miller, F. Kuster, D. Brabazon, I. Naydenova, *Polymers (Basel)* **2022**, *14*, 1858.
[14] a) A. G. Mayes, J. Blyth, R. B. Millington, C. R. Lowe, *Anal. Chem.* **2002**, *74*, 3649; b) N. Jiang, H. Butt, Y. Montelongo, F. Liu, S. Afewerki, G.-L. Ying, Q. Dai, S.-H. Yun, A. K. Yetisen, *Adv. Funct. Mater.* **2018**, *28*, 1702715.
[15] S. Davies, Y. Hu, J. Blyth, N. Jiang, A. K. Yetisen, *Adv. Funct. Mater.* **2023**.
[16] S. Davies, Y. Hu, N. Jiang, Y. Montelongo, A. Richardson, J. Blyth, A. K. Yetisen, *Biosens. Bioelectron.* **2022**, *207*, 114206.
[17] R. Ahmed, A. K. Yetisen, S. H. Yun, H. Butt, *Light: Sci. Appl.* **2017**, *6*, 16214.
[18] T. Mishina, M. Okui, F. Okano, *Appl. Opt.* **2002**, *41*, 1489.
[19] A. K. Yetisen, H. Butt, S.-H. Yun, *ACS Sens.* **2016**, *1*, 493.
[20] N. J. Trengove, S. R. Langton, M. C. Stacey, *Wound Repair Regen* **1996**, *4*, 234.
[21] Y. Zhang, Y. Hu, N. Jiang, A. K. Yetisen, *Biosens. Bioelectron.* **2022**, *219*, 114825.
[22] J.-P. Berenger, *J. Comput. Phys.* **1994**, *114*, 185.